RSC Advances

ROYAL SOCIETY OF CHEMISTRY

www.rsc.org/advances

Coupling FtsZ filaments and morphodynamics during bacterial cell divisions

Zhuan Liu[1] and Kunkun Guo[a1]

[1] *College of Materials Science and Engineering, Hunan University, Changsha, 410082, China*

(Dated: October 16, 2014)

FtsZ filaments play a central role in bacterial cell division. A theoretical framework by combining phase field model for rod-shaped cells with a kinetic description for FtsZ ring maintenance, is developed to investigate cell morphodynamics during bacterial cell division. The cell division time and cell shape are collectively determined by the curvature elastic energy of cell membrane/wall and the constriction force generated by FtsZ rings. The dependences of cell morphodynamics during cell division on different initial states of rod-shaped cells and FtsZ rings, such as the aspect ratio and the FtsZ concentration in cells, Z_{T}, are extensively studied. The obtained results with the measured experimental parameters are found to be well comparable to the observed results physiologically. Likewise, it is found that the quasi-steady state of FtsZ rings accords with the theoretical result derived from the kinetic description of FtsZ rings. In addition, morphological phase diagram is presented as functions of the FtsZ concentration in cells, Z_{T}, and aspect ratio of rod-shaped cells, giving that rod-shaped cells with high Z_{T} or/and aspect ratio tend to divide. It will be straightforward to extend the theoretical framework to other complicated systems relevant to filamentous proteins and cells, for example, maintaining structural integrity, serving as a template for cell growth, cell adhesion and motility, and mechanical signal transduction.

[a] To whom correspondence should be addressed. Email:kunkunguo@hnu.edu.cn

Cell morphodynamics during bacterial cell divisions is extensively investigated by a combination of phase field model for rod-shaped cells and a kinetic description for FtsZ ring maintenance.

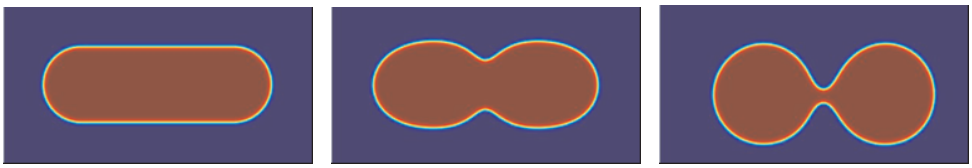

t=0 s, $R = 0.5$ μm t=6.4 s, $R = 3.3$ μm t=160 s, $R = 0.095$ μm

I. INTRODUCTION

Filamenting temperature sensitive mutant Z (FtsZ) protein is GTPase[1], i.e. it binds guanosine triphosphate (GTP) and hydrolyzes it to guanosine diphosphate (GDP)[2–4]. Under different *in vitro* experimental conditions, FtsZ proteins in the presence of GTP can assemble into a large variety of dynamic structures, such as short filaments, bundles, ribbons, minirings, helices and tubes[5–9]. A typical length of short FtsZ filaments as observed experimentally at the physiological concentration is about 125 nm that generally consists of 30 FtsZ monomers[10]. FtsZ filaments play an important role in providing mechanical stability and defining the bacterial shapes, for example, cell division in E. Coli and other rod-like bacteria[11]. FtsZ filaments assemble into a thin ring in the midcell region (the bacterial cell-division site). The thin ring called FtsZ ring recruits other proteins to form the septal ring that exerts the force to divide the cell. However, the mechanism remains unclear how the dynamic FtsZ ring forms underlying the cell membrane and plays a central role in the force generation during cell divisions[12].

The FtsZ ring has a dynamic structure, where filaments assemble into the ring and disassemble from it[13]. The mechanism of its dynamic behavior can not be completely explained by the dynamic instability of microtubule or treadmilling of other filamentous proteins[14,15]. Of course, the GDP-bound FtsZ monomers that have been depolymerized from the FtsZ ring, could be rapidly exchanged into GTP-bound ones in the cytoplasm for subsequent polymerizations, thereby giving that cytosolic filaments consist entirely of GTP-bound monomers. Likewise, FtsZ monomers are observed to be rapidly exchanged between FtsZ rings and the cytoplasmic pool, and a half time of turnover is measured experimentally about 10 s[16].

One mechanism for force generations is proposed in several theoretical models, arising from curvature transitions induced by GTP hydrolysis[5,7–9,17–20]. However, the conformation switch is observed experimentally to be independent of their nucleotide binding states. At the same time, crystal structures of single FtsZ monomers reveal the structure of GTP-bound monomer similar to GDP-bound one[17]. Subsequently, the effects of nucleotide binding on the structure of a FtsZ dimer are extensively studied by molecular dynamic simulations, supposing that the FtsZ-dimer structure depends on their nucleotide binding states[18]. As a

whole, in the presence of GTP hydrolysis, FtsZ filaments are expected to possess three different curved conformations[5,7–9,19,20]. The first is a straight conformation with a curvature radius larger than 0.5 μm when FtsZ protein binds GTP molecules. The intermediate curved conformation corresponds to a 2.5 degree bend between monomers, producing a curvature radius about 200 nm. Finally, the highly curved conformation (miniring) contains 16 monomers bound to GDP molecules with a 23 degree bend at each interface, and its intrinsic curvature radius ranges from 12.5 to 100 nm. Therefore, the coupling of GTP hydrolysis at each FtsZ monomers within the FtsZ filament could cause a transition from a straight conformation to a curved one, by which the FtsZ filament would provide the force to constrict the cell wall/membrane.

A completely different mechanism for force generation has been suggested in other theoretical models[21–24]. These models propose that FtsZ ring consists of several short filaments, and these short filaments can interact with each other *via* lateral and longitudinal bonds. These lateral and longitudinal bonds provide a negative (favorable) free energy. Meanwhile, a constriction force would be generated as the cooperativity of the polymerization, the condensation and bundling of FtsZ filaments proceed, together with the increased number of lateral and longitudinal bonds.

So far, force generation of FtsZ rings is mainly focused regardless of shape transformations of cells. Whereas, the coupling of FtsZ rings and cell shape is expressed in such a way that the constriction force is a free parameter independent of the dynamic turnover of FtsZ rings[25]. Phase field method has a reputation to be very general and applicable to complex microstructural phenomena, as well as has been extended to study vesicle shape dynamics recently[26–29], in particular, cell morphodynamics due to phase transitions between cross-linked actin filaments and bundles[30,31]. In the present study, one theoretical framework is firstly developed to study the coupling of cells and FtsZ rings system, and combines a kinetic description of FtsZ-ring maintenance with phase field dynamics for cell morphodynamics. The most advantage of the theoretical framework is to capture the collective behaviors of shape transformations of cells and the constriction forces generated by dynamic FtsZ rings. Furthermore, this theoretical framework presented here is easily extended to investigate other complicated systems relevant to filamentous proteins and cells.

This paper is organized as follows. Section II contains a detailed description of the theoretical framework

by combination of phase field model for cells and one kinetic model for FtsZ-ring turnover, together with the numerical calculation method for the combined theoretical model. In section III, a typical dynamic process during bacterial cell division is presented, and the steady states of cells are discussed as functions of different initial states of cells and FtsZ rings, such as the total concentration of FtsZ in cell, the total number of FtsZ monomers within the ring, the total number of FtsZ-GDP monomers within the ring, the initial mean length of FtsZ filaments within the ring, λ, and the aspect ratio of cells. Additionally, morphological phase diagram is presented as functions of the total concentration of FtsZ in cell and the aspect ratio of cells. Finally, a brief summary and outlook are given in section IV.

II. THEORETICAL METHOD

Our model is motivated by experiments on E. Coli and FtsZ ring where cell division for E. Coli is observed in the presence of FtsZ ring in the midcell[11]. Therefore, one new theoretical framework that couples cell division of bacteria with force generation of FtsZ ring, is developed to study dynamic processes of cell divisions and changes of constriction forces. Phase field model that can avoid to track the explicit boundary and has been successfully applied to solve free-boundary problems[26–30], has been widely used to study cell morphodynamics. At the same time, a kinetic description of FtsZ-ring maintenance has been developed[13], including the incorporation of new short filaments into the ring, GTP hydrolysis in the ring and rapidly nucleotide exchange in the cytoplasmic pool, disassembly of GDP-bound monomers within the ring, and the mechanical characterization of GDP-bound monomers in FtsZ ring. However, the disassembly of GTP-bound monomers and the contribution of GTP-bound monomers within the ring to the constriction force are neglected in the previous work[13]. In this, it is the first time to combine phase field model with the kinetic description of FtsZ rings, including the effect of GTP-bound monomers within the ring.

A typical bacteria, such as E. Coli, is approximately assumed as a two-dimensional rod-shaped cell with a fixed surface area A_0, as volume in three-dimension, and the dynamic turnover of short FtsZ filaments is considered to couple with GTP hydrolysis, see Fig. 1. The FtsZ ring that consists of several short FtsZ filaments, as expected, is always distributed in the midcell. In order to distinguish the interior and exterior

of the rod-shaped cell, an auxiliary phase field, ϕ, is introduced, where ϕ takes on 1 in the interior of the cell wall but $\phi = 0$ in the cell exterior. This field varies abruptly in the diffusive interface between two limited values, $\phi = 1$ and $\phi = 0$. The width of this interface, ϵ, is used to describe the thickness of cell wall.

FIG. 1. (color online) (a) The schematic illustration of a rod-shaped cell with FtsZ rings located in the middle of cell along the horizontal direction, where the yellow color indicates the diffusion interface with a width of ϵ, the grey color is the interior of the cell, $\phi = 1$, while white with $\phi = 0$, and green is FtsZ ring located in the middle of rod-shaped cell. (b) Enlarged view of the FtsZ ring in midcell that consists of short FtsZ filaments.

Therefore, the dynamic evolution equation for the phase field is given by[26,27,30]

$$\frac{\partial \phi}{\partial t} = -\mathbf{u} \cdot \nabla \phi + \Gamma[\epsilon \nabla^2 \phi - \frac{G'}{\epsilon} + \epsilon c |\nabla \phi|] \tag{1}$$

where the advection term couples the phase field to the local flow velocity, $\mathbf{u}$, the parameter ϵ controls the width of the cell wall, Γ is a parameter, the local curvature is denoted by $c = -\nabla \cdot \frac{\nabla \phi}{|\nabla \phi|}$, and $G = 18\phi^2(1-\phi^2)$ is a double well potential with minima at $\phi = 1$ and $\phi = 0$.

In the present study, the shape of cell membrane or cell wall can be determined by the cooperations of various forces, including the surface tension, the bending force, and the pressure that constrains the cell area of vesicles, as volume in three dimensions. In addition, the perimeter of the cell wall is observed experimentally not to be fixed[33], allowing proteins or lipid molecules to enter or escape during either cell wall expansion or cell divisions. It is also considered for the radial and constriction forces generated from FtsZ rings in the midcell, and the effective friction caused by cell divisions and cell motile. At first, the surface energy that is proportional to the cell's perimeter L, is able to be implemented in the phase-field formulations as follows[28,29]

$$H_{\text{te}} = \gamma L = \gamma \int (\frac{\epsilon}{2} |\nabla \phi|^2 + \frac{G}{\epsilon}) d\mathbf{r} \tag{2}$$

where γ is the surface tension. Then, the area density of surface tension force is derived as follows

$$\mathbf{F}'_{\rm te} = -\frac{\delta H_{\rm te}}{\delta \mathbf{R}} = \frac{\delta H_{\rm te}}{\delta \phi}\nabla\phi = -\gamma(\epsilon\nabla^2\phi - \frac{G'}{\epsilon})\nabla\phi. \tag{3}$$

Here, this area density can be converted into a line density with $\mathbf{F}'d\mathbf{r} = \mathbf{F}_{\rm te}\epsilon|\nabla\phi|^2 d\mathbf{r}$[30]. Therefore, the surface tension force with a line density is deduced as

$$\mathbf{F}_{\rm te} = -\gamma(\nabla^2\phi - \frac{G'}{\epsilon^2})\frac{\nabla\phi}{|\nabla\phi|^2} \tag{4}$$

The bending energy $H_{\rm be}$ of the cell wall[32] is written in the phase field formulation as

$$H_{\rm be} = \frac{\kappa}{2}\int \frac{1}{\epsilon}[\epsilon\nabla^2\phi - \frac{G'}{\epsilon}]^2 d\mathbf{r} \tag{5}$$

where κ is the bending rigidity of the cell wall. Note that the spontaneous curvature is taken to be zero. The area density of the bending force can be derived and converted into a line density as above. The bending force with a line density is given as follows[30]

$$\mathbf{F}_{\rm be} = \kappa(\nabla^2 - \frac{G''}{\epsilon^2})(\nabla^2\phi - \frac{G'}{\epsilon^2})\frac{\nabla\phi}{|\nabla\phi|^2}. \tag{6}$$

The cell area in two dimension, as volume in three dimension, $A = \int \phi d\mathbf{r}$ is observed experimentally[33] to be conserved during cell divisions, indicating that perimeter is not highly conserved. Therefore, a constraint term is required to guarantee the cell area and can be expressed in the form of of phase field

$$H_{\rm ar} = -\frac{M_A}{2}(A(\phi) - A_0)^2 \tag{7}$$

where M_A is large and A_0 is the prescribed area. The force derived by the constraint term is

$$\mathbf{F}_{\rm ar} = M_A(\int \phi d\mathbf{r} - A_0)\frac{\nabla\phi}{|\nabla\phi|}. \tag{8}$$

The coupling of FtsZ rings with cells provides a retraction force to cell wall/membrane, thereby leading to cell divisions. In order to simply describe the mechanical property of the FtsZ ring, a stable and smooth FtsZ ring is assumed to form in the midcell. This assumption of a smooth ring is justified by the mechanical averaging across the thickness of the ring due to the uniform distribution of hydrolyzed and unhydrolyzed

monomers. The mechanical energy H_z stored in the FtsZ ring as functions of its radius and FtsZ monomers is assumed to obey with linear elasticity, giving by[34]

$$H_z = \frac{1}{2}\int B\left(\kappa(s) - \frac{1}{R}\right)^2 ds = \frac{B\delta}{2}\left((S - S_D)(\kappa_T - \frac{1}{R})^2 + S_D(\kappa_D - \frac{1}{R})^2\right) \quad (9)$$

where B is the bending modulus of a FtsZ filament. $\kappa(s)$ is the preferred curvature as a function of the position in the ring (s) and is defined piecewise as either κ_T or κ_D dependent of the hydrolysis state of that position (GTP- or GDP-bound respectively) in the ring. δ is the size of a FtsZ monomer and R is the radius of the ring or the radius of the midcell. S and S_D are the total number of FtsZ monomers and GDP-bound FtsZ monomers within the ring, respectively. Performing the derivative of the mechanical energy with respect to radius, R, the radial force generated by the ring is given by

$$\mathbf{F}_z = -\frac{\delta H_Z}{\delta R}\cdot\mathbf{n} = \frac{B\delta S}{R^3}(R\kappa_T - 1 - \frac{S_D}{S}(\kappa_T - \kappa_D)R)\frac{\nabla\phi}{|\nabla\phi|} \quad (10)$$

where $\mathbf{n}$ denotes the generated force along the normal direction to the cell wall.

In order to achieve the mechanical energy, H_z, of FtsZ-ring given by the equation (9), the total number of FtsZ monomers and GDP-bound FtsZ monomers within the ring have to be obtained in advance. This involves a kinetic description of FtsZ ring turnover, including the incorporation of free short filaments and FtsZ monomers into the ring, hydrolysis of GTP-bound monomers within the ring, disassembly of both GTP-bound and GDP-bound monomers at the tip of the filament within the ring, as well as the mechanical characterization of the FtsZ-ring served as force generation. Compared to the previous kinetic model proposed by Cytrnbaum[13], the contributions of GTP-bound monomers within the ring to disassembly and to force generation are considered. Two main physical quantities are introduced, and they are the length distribution of filaments in the ring, $p(l,t)$, and the number of hydrolyzed monomers, $S_D(t)$ in the ring, where l is the number of monomers within the filament at time t. Subsequently, the total number of FtsZ monomers, S, and filament tips, F, in the ring can be derived by $S = \int_0^\infty lp(l,t)dl$ and $F = \int_0^\infty p(l,t)dl$, respectively. The cytosolic concentration of FtsZ monomers can be obtained from $Z_T - S/(N_c A)$, where Z_T is the total concentration of FtsZ monomers in the cell, and the factor $N_c A$ is used to transform the number of molecules to concentration in micromoles.

The cytosolic filaments are experimentally observed to satisfy with an exponential distribution when the

cytosolic concentration is above the critical concentration[10]. As concluded from the polymer dynamics independent of cooperative versus isodesmic assembly or the fragmentation and annealing, filament lengths are also found to obey a quasi-steady exponential distribution with a mean length, λ[13]. Therefore, the lengths of cytosolic filaments are reasonably assumed to possess an exponential distribution with a mean length of $\lambda = 30$ monomers (typical length), and its amplitude can be determined by the cytosolic concentration. The incorporation rate of filaments with a length, l, is proportional to the cytosolic concentration of the same filament length. In addition, the GDP-bound monomers depolymerized from the ring could be rapidly exchanged into GTP-bound monomers, thereby giving that cytosolic filaments consist entirely of GTP-bound monomers. As previously presented[14,15], the depolymerization of one monomer is governed by not only its position within a filament but also nucleotide state. $\kappa_{\rm off}^{\rm T}$ and $\kappa_{\rm off}^{\rm D}$ are defined as the depolymerization rates of GTP-bound and GDP-bound FtsZ monomers at the filament tips, respectively. However, the GDP-bound monomers at the filament tips are experimentally found to disassemble more rapidly than GTP-bound ones[4]. The fraction of GDP-bound monomers in the ring has the form of $f_{\rm D} = S_{\rm D}/S$.

Filaments are assumed to be randomly distributed throughout the ring. Changes in the length distribution $p(l,t)$ arise from the incorporation of both FtsZ filaments and free monomers in the cytosol, and the disassociation of monomers from filament tips dependent of their nucleotide states. Therefore, the filament length distribution $p(l,t)$ in the ring obeys with

$$\frac{\partial p(l,t)}{\partial t} = 4\pi R\kappa_{\rm in}(Z_{\rm T} - \frac{S}{N_c A})\frac{1}{\lambda}\exp\left(-l/\lambda\right) + [\kappa_{\rm off}^{\rm T}(\frac{S-S_{\rm D}}{S}) + \kappa_{\rm off}^{\rm D}(\frac{S_{\rm D}}{S})][p(l+1,t) - p(l,t)] \qquad (11)$$

where, $4\pi R$ is the number of available binding sites in which new filaments or free monomers can only associate along the outer edges of the FtsZ ring, and $\kappa_{\rm in}$ is the membrane associate rate.

The time evolution of the number of GDP-bound FtsZ monomers in the ring, $S_{\rm D}$, is given by

$$\frac{\partial S_{\rm D}}{\partial t} = \kappa_{\rm hy}(S - S_{\rm D}) - \kappa_{\rm off}^{\rm D}\frac{S_{\rm D}}{S}F \qquad (12)$$

The first term of the right side in Eq. (12) accounts for the hydrolysis that any GTP-bound monomers in the FtsZ ring can hydrolyze in a stochastic manner independent of the state of adjacent monomers. The second term of the right side in Eq. (12) accounts for the disassembly of GDP-bound monomers at all filament tips within the ring F. The total number of filament tips F is obtained by integrating the length distribution of

filaments within the ring as presented in the preceding paragraph. $\kappa_{\rm hy}$ is the rate of GTP-bound monomers hydrolyzed into GDP-bound ones. By combining Eq. (11) and (12), the quasi-steady state for this subsystem (FtsZ ring) is given by the following

$$S_{\rm qss} = \frac{4\pi R N_c A Z_T \kappa_{\rm in} \lambda^2 (\kappa_{\rm off}^D + \kappa_{\rm hy}\lambda)}{4\pi R\lambda^2 \kappa_{\rm in}(\kappa_{\rm off}^D + \kappa_{\rm hy}\lambda) + \kappa_{\rm off}^D N_c A(\kappa_{\rm off}^T + \kappa_{\rm hy}\lambda)} \tag{13}$$

$$S_{\rm Dqss} = \frac{4\pi R N_c A Z_T \kappa_{\rm in} \lambda^3 \kappa_{\rm hy}}{4\pi R\lambda^2 \kappa_{\rm in}(\kappa_{\rm off}^D + \kappa_{\rm hy}\lambda) + \kappa_{\rm off}^D N_c A(\kappa_{\rm off}^T + \kappa_{\rm hy}\lambda)} \tag{14}$$

$$f_{\rm Dqss} = \frac{S_{\rm Dqss}}{S_{\rm qss}} = \frac{\lambda \kappa_{\rm hy}}{\kappa_{\rm off}^D + \kappa_{\rm hy}\lambda} \tag{15}$$

$$p_{\rm qss}(l) = \frac{S_{\rm qss}}{\lambda^2} e^{-l/\lambda} \tag{16}$$

where the subscript (qss) indicates the parameters at the quasi-steady state. It suggests from the quasi-steady state, Eqs. (13)-(16), that the fraction of hydrolyzed monomers in the ring at the steady state, $f_{\rm Dqss}$, that is, the ratio of $S_{\rm D}$ to S, is independent of the radius, R, and attains a theoretical value of $f_{\rm Dqss} = 0.02$, and the filament length in the ring is deduced to obey with an exponential distribution relevant to the total number of FtsZ monomers in the ring, $S_{\rm qss}$.

During cell divisions, an effective friction between cell wall/membrane and fluid environment is proportional to the local speed, $\mathbf{u}$, obeying with $\mathbf{F}_{\rm fr} = -\tau\mathbf{u}$. At the quasi-steady state, the total force approaches zero, that is $\mathbf{F}_{\rm te} + \mathbf{F}_{\rm be} + \mathbf{F}_{\rm ar} + \mathbf{F}_{\rm z} + \mathbf{F}_{\rm fr} = 0$. Therefore, the evolution equation of phase field model in the presence of FtsZ rings according to Eqs (1)-(10) can be derived as follows

$$\begin{aligned}\frac{\partial \phi}{\partial t} = &-\frac{1}{\tau}\{\kappa(\nabla^2 - \frac{G''}{\epsilon^2})(\epsilon\nabla^2\phi - \frac{G'}{\epsilon}) - \gamma(\epsilon\nabla^2\phi - \frac{G'}{\epsilon}) + M_A(A(\phi) - A_0)|\nabla\phi| \\ &+\frac{B\delta S}{R^3}(R\kappa_{\rm T} - 1 - \frac{S_{\rm D}}{S}(\kappa_{\rm T} - \kappa_{\rm D})R)|\nabla\phi|\} + \Gamma[\epsilon\nabla^2\phi - \frac{G'}{\epsilon} + \epsilon c|\nabla\phi|]\end{aligned} \tag{17}$$

Due to the presence of MinCDE proteins in cells, spatial distributions of FtsZ rings are regulated to locate in the middle of of cells[1,35]. FtsZ ring that generally consists laterally of 6-10 filaments, localizes in the midcell along the horizontal axis at a wide range of 25 nm[11]. Therefore, the force generated by FtsZ rings

in other positions is very small, and can be approximately neglected. The evolution equation of phase field model in absence of FtsZ rings is given by

$$\frac{\partial \phi}{\partial t} = -\frac{1}{\tau}\{\kappa(\nabla^2 - \frac{G''}{\epsilon^2})(\epsilon\nabla^2\phi - \frac{G'}{\epsilon}) - \gamma(\epsilon\nabla^2\phi - \frac{G'}{\epsilon}) + M_A(A(\phi) - A_0)|\nabla\phi|\} + \Gamma[\epsilon\nabla^2\phi - \frac{G'}{\epsilon} + \epsilon c|\nabla\phi|] \quad (18)$$

The fourth order nonlinear partial differential equations (17) and (18) are solved using an alternating direction implicit scheme and a second order backward differentiation formula, while the partial differential equations (11) and (12) are explicitly solved using a forward Euler differential scheme. These position-dependent equations are solved on a 400×200 rectangle with the box size of $40r_0 \times 20r_0$, where the unit length r_0 is about 0.1 μm. Therefore, the physical size of the box is about 3 μm, which is available to *in vivo* bacteria[1,11]. The simulation time step of these evolution equations is $\Delta t = 4.0 \times 10^{-5}$ s. A typical simulation starts with a stationary rod-shaped cell with surface area $A_0 = 2.78$ μm^2 and aspect ratio equal to 3.0, which are also comparable to *in vivo* bacteria [1,11]. The diffusive interface that describes the thickness of cell wall, is chosen as one unit length, $r_0 = 100$ nm, which is comparable to the experimental observed thickness of cell wall in the range from 20 to 50 nm[11]. Compared with the experimental result for the lateral size of FtsZ rings[11], the dynamic FtsZ ring is assumed to be distributed in the middle of a rod-shaped cell, and has a width of 0.3 r_0 (about 30 nm). Therefore, the evolution equation of phase field in the presence of the force generated by FtsZ rings, Eq. (17), is only solved on three grid sizes (about 30 nm) in the middle of a rod-shaped cell. The lengths of FtsZ filaments are presented to satisfy with a quasi-steady exponential distribution: $1/\lambda \cdot e^{-l/\lambda}$, see Eq. (16), where λ is the mean length of FtsZ filaments. Therefore, the total number of the monomers within the ring at the initial state is obtained by $S_{\text{initial}} = \int lp(l,0)dl$. Likewise, the filament length distribution within the ring is deduced by $p(l,0) = S_{\text{initial}}/\lambda^2 \cdot e^{-l/\lambda}$ in the initial state. The length distribution and the total number of GDP-bound FtsZ monomers within the ring for the next time step are able to be obtained according to the evolution of equations (11) and (12). The resulting values of S and S_{D} are inserted into the evolution equations (17)-(18) of phase field model to produce a new shape of a cell. These equations are solved iteratively to produce the new cell shape, as well as the updated distribution of FtsZ filaments. The steps are finished until a steady state is eventually reached where the cell has a stationary shape and FtsZ filaments possess a stable distribution. The parameters used in the numerical calculations that are all comparable to the experimental values[13,31], are provided in Table I.

TABLE I. Model parameters.

	Description	Value
γ	Surface tension	50 pN/μm
κ	Bending rigidity	0.5 pNμm
τ	Friction coefficient	5×10^3 pN s/μm^3
B	Bending modulus of FtsZ filament	1.2 $\times10^{-2}$ pNμm^2
ϵ	boundary width	0.1 μm
δ	Size of FtsZ monomer	4 nm
Γ	Parameter	0.1
κ_{T}	Intrinsic curvature of GTP-bound FtsZ	0.8 μm^{-1}
κ_{D}	Intrinsic curvature of GDP-bound FtsZ	80 μm^{-1}
N_{c}	Conversion factor	600 μM$^{-1}\mu$m^{-3}
κ_{in}	Membrane association rate	0.0021 μM$^{-1}\mu$m^{-1}s^{-1}
$\kappa_{\mathrm{off}}^{\mathrm{T}}$	Depolymerization rate of GTP-bound FtsZ	0.1 s^{-1}
$\kappa_{\mathrm{off}}^{\mathrm{D}}$	Depolymerization rate of GDP-bound FtsZ	3.5 s^{-1}
κ_{hy}	GTP hydrolysis rate	0.03 s^{-1}
M_{A}	Area constraint	1.0 pN/μm^2
λ	Average number of monomers in a filament	30 monomers
Z_{T}	Total concentration of FtsZ monomers in cell	13 μM

III. RESULTS AND DISCUSSIONS

A. Dynamic process for cell division

A typical FtsZ ring has been reported that approximately 30% of the total FtsZ monomers are found within FtsZ rings in *in vivo* cells[16]. According to the concentration presented in Tab. I, we find that the total number of FtsZ monomers within the ring about 30% of Z_{T} is $S = 5504$ monomers, which is the same magnitude of the 5000-15000 FtsZ monomers estimated to be present in bacterial cells[16]. Figure 2 presents an example for the particular set of parameter values given in Table I. The cell's area, as volume in three

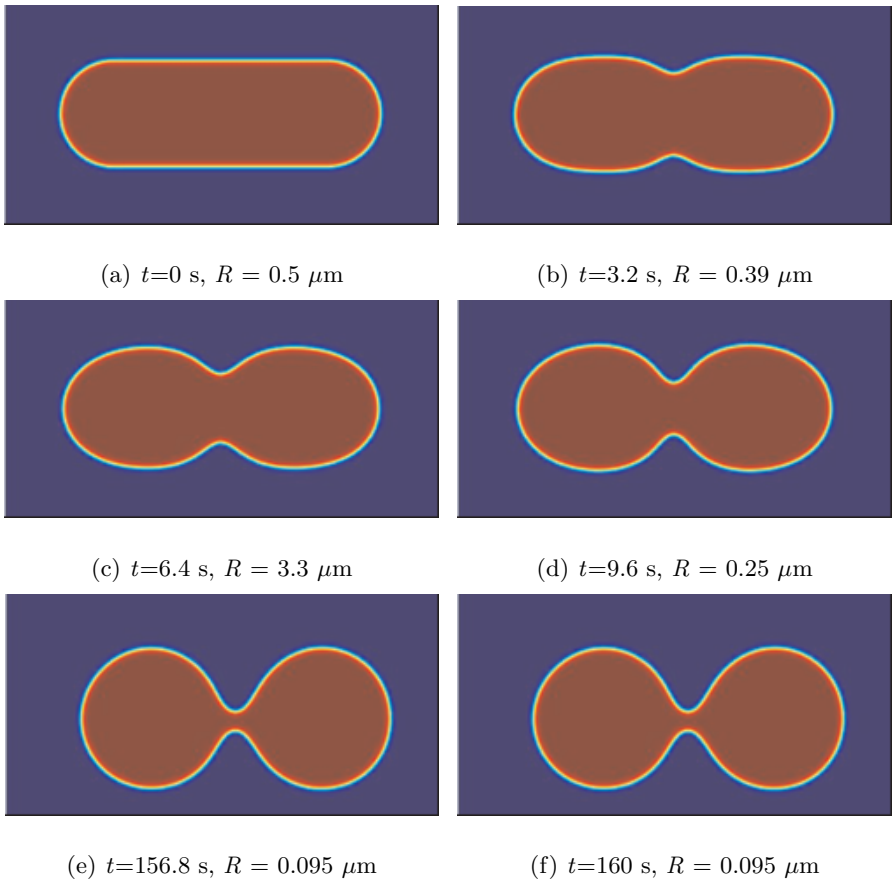

(a) t=0 s, R = 0.5 μm (b) t=3.2 s, R = 0.39 μm

(c) t=6.4 s, R = 3.3 μm (d) t=9.6 s, R = 0.25 μm

(e) t=156.8 s, R = 0.095 μm (f) t=160 s, R = 0.095 μm

FIG. 2. (color online) . Snapshots of the numerical evolution of a cell shape during cell division.

dimension, is found to be changed less than 0.15% throughout the dynamic process. It is seen from these snapshots that a cell starting with a rod-shaped cell at a radius, R, of 0.5 μm retracts in the midcell down to a radius about 0.095 μm at the simulation time t = 160 s, and then maintains this shape for a long time eventually to reach the steady state. The time for achieving this deformation has the same magnitude with the contraction time of minutes as experimentally observed in live cells[11]. Several physical quantities, such as the constriction force generated by FtsZ-rings, the total number of FtsZ monomers, S, and GDP-bound FtsZ monomers, S_{D}, within the ring, the fraction of hydrolyzed monomers in the ring, f_{D}, and length distributions $p(l,t)$, are thoroughly studied during the dynamic process of cell divisions. We find that the constriction force at first shifts from 28 pN to 48 pN along with the decrease of the radius at the midcell, R, down to 25 nm, and then drops to 32 pN with further decrease of R to 10 nm. The obtained constriction force has the same magnitude with the previous result that cell division can succeed for a wide range of FtsZ rings force between 8 pN and 80 pN[25]. Along with the process of cell divisions, the total number of FtsZ monomers,

S, GDP-bound FtsZ monomers, $S_{\rm D}$, and the fraction of hydrolyzed monomers in the ring, $f_{\rm D}$, are found to achieve their stable values till the cell reaches the steady sate, where S is equal to 2643 ± 20 monomers, $S_{\rm D}$ is 421 ± 5 monomers and $f_{\rm D}$ is 0.1610, respectively. They are close to the theoretical values, $S_{\rm qss} = 3235 \pm 150$ monomers, $S_{\rm Dqss} = 661 \pm 30$ monomers and $f_{\rm Dqss} = 0.204$ derived from Eqs. (13)-(15). Likewise, the fraction of hydrolyzed monomers in the ring is well consistent with the value as observed experimentally[10] about 20 %. In addition, we find that the length distributions, $p(l,t)$, for FtsZ rings whether in the initial state or steady state, satisfy the exponential distributions with the characteristic length about 30 monomers.

B. The effect of initial states

The distribution of cytosolic FtsZ filaments as observed in FRAP experiments, is found to be well consistent with the theoretical prediction for an exponential length distribution[10]. Likewise, both the mean length and its amplitude are found to be determined by the current cytosolic concentration[10], where the cytosolic concentration is well above the critical concentration. Figure 3 gives the effect of the mean length for FtsZ filaments, λ, on the dynamic process during cell divisions. The particular set of parameter values is given in Table I, and several physical quantities at the steady state, such as S, $S_{\rm D}$, $f_{\rm D}$ and R, are listed in Fig. 3. Figure 3(a) presents the dependences of the constriction forces generated by FtsZ rings at the initial state and steady state, $F_{\rm z,initial}$ and $F_{\rm z,final}$, on λ. It is found that the constriction forces generated by FtsZ rings at the initial state maintain approximately to 28.53 pN, and are independent of the mean length for FtsZ filaments, λ. This result is attributed by the number of GTP-bound and GDP-bound FtsZ monomers within the rings kept constant at the initial state. Whereas, the constriction forces at the steady state at first increase slowly, and then increase abruptly as a function of the mean length, λ. At $\lambda = 30$ monomers, the constriction force increases up to 32.81 ± 0.92 pN, close to the force required to cell division. Likewise, we find in the inset of Fig. 3(a) that the contraction rates, dR/dt, approach zero when the mean length, λ, is less than 24 monomers. Likewise, it can be concluded from Eq. (11) that the smaller mean length, the less value of $p(l,t)$, and the corresponding total number of FtsZ and GDP-bound FtsZ monomers within the ring, S and $S_{\rm D}$, are relatively small at the steady state, thereby leading to the reduction of constriction forces. In

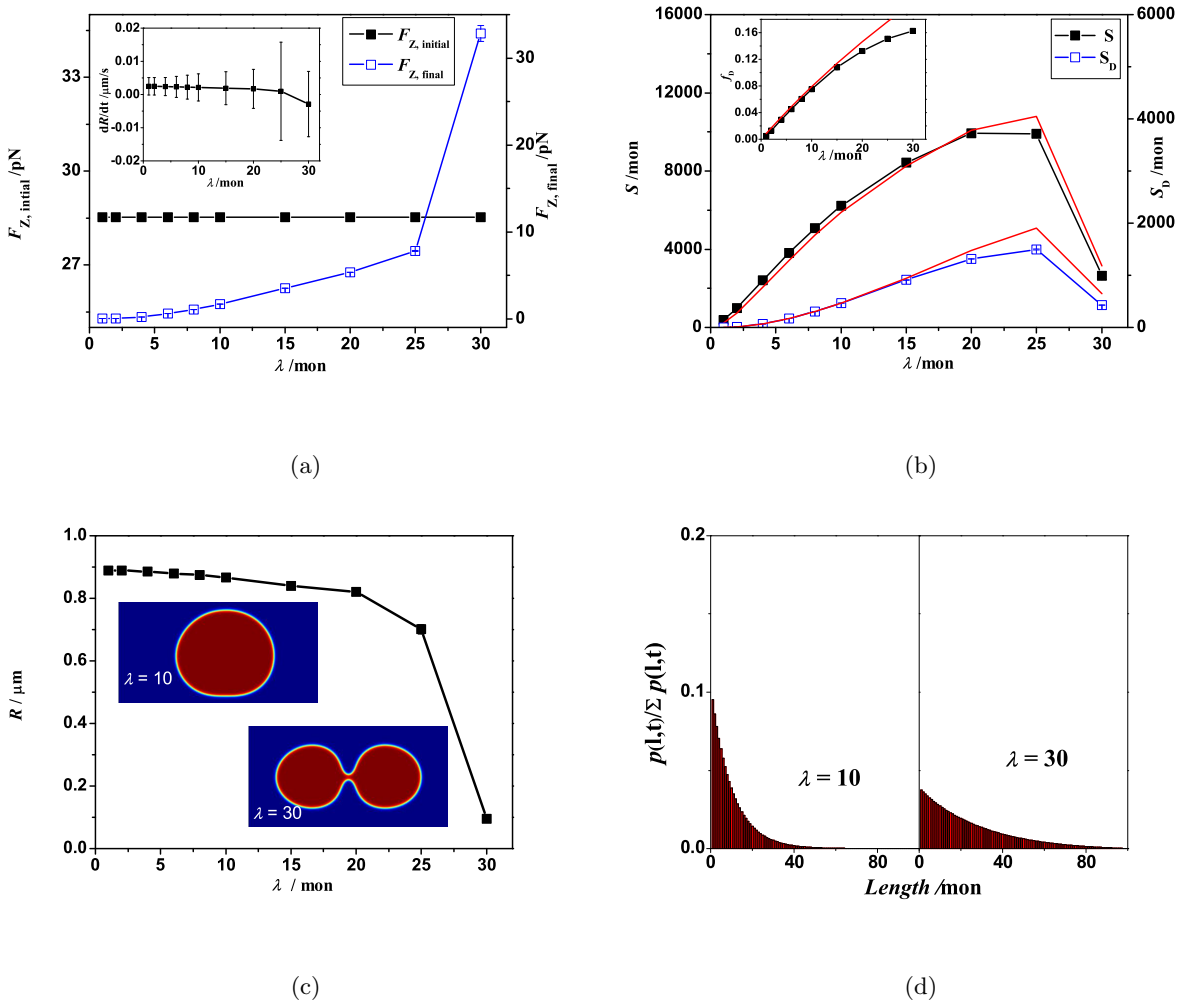

FIG. 3. (color online) . The effect of the mean length for FtsZ filaments, λ, (a) constriction forces generated by FtsZ rings at the initial and steady state, and contraction rates in the inset, (b) S, S_{D} and f_{D} at the steady state, the red lines are obtained from the theoretical values, Eqs. (13)-(15),(c) The radius of the constriction ring at the steady state, a cell shape at the steady state given in the inset, (d) Length distribution with $\lambda = 10$ and $\lambda = 30$ at the steady state.

addition, it is seen from Fig. 3(b) that the total number of FtsZ and GDP-bound FtsZ monomers within the ring at the steady state, S and S_{D}, would be enhanced along with the increase of the mean length, however, they start to slightly decrease when the radius at the midcell rapidly retracts. At the same time, it is found in the inset of Fig. 3(b) that the fraction of hydrolyzed monomers in the ring, f_{D}, ranges from 0.0752 to 0.01626 when the mean length of FtsZ filaments shifts from 1 to 30 monomers. Additionally, the total number of FtsZ and GDP-bound FtsZ monomers, S and S_{D}, and the fraction of hydrolyzed monomers in the ring, f_{D},

obtained in the numerical calculation (solid symbols) are found to be comparable to the theoretical curves derived from Eqs. (13)-(15) (red line). Likewise, the length distributions of FtsZ filaments at the steady state are presented in Fig. 3(d), where the mean lengths of FtsZ filaments are initially chosen as 10 and 30 monomers, respectively. The distributions of FstZ filaments are found to satisfy exponential distributions with their characteristic lengths close to the preset mean lengths. As a result, these results reveal that cell division depends on the mean length of FtsZ filaments, because the total number of FtsZ and GDP-bound FtsZ monomers, S and S_{D}, and the fraction of hydrolyzed monomers in the ring, f_{D}, would be changed as a function of the mean length of FtsZ filaments, thereby leading to the alteration of the constriction forces generated by FtsZ filaments within the ring.

Cell wall expansion is experimentally observed to be mainly contributed by cell-wall biosynthesis, such as peptidoglycan synthesis proteins.[36,37] Meanwhile, the turgor pressure is found not to be required for cell-wall biosynthesis, but does play a simple role whereby it stretches recently assembled, unextended peptidoglycan[36,37]. Once the FtsZ-ring is formed and is anchored to cell wall/membrane, other proteins, such as the septum synthesis proteins, are recruited to the ring site, as well as cell wall growth and remodeling can proceed. In addition, many bacteria, for example, E. coli, generally elongate with both an exponential growth and a constant diameter. Therefore, the dynamic processes of cell divisions and steady states of cells are extensively investigated in response to the preset aspect ratio for rod-shaped cells. Then, the results are given in Figure 4. The cell area of rod-shape cells, as expected, is altered upon the change of the aspect ratio. However, the initial concentration of FtsZ monomers in cells is chosen as a constant, 13 μM, the fraction of FtsZ monomers within the ring contains 30 % of the total number of FtsZ monomers, and the fraction of hydrolyzed monomers in the ring, f_{D}, is 0.4. As shown in Fig. 4(c), when the aspect ratio for rod-shaped cells shifts from 1.6 to 3.8, the radius at the midcell in the steady state, R, at first increases from 0.5 μm close to 1.0 μm that possesses one spherical shape, and then decreases gradually until cell division finishes. Typical shapes of cells at the initial and steady state are given in the inset of Fig. 4(c) and their aspect ratio are 2.4 and 3.8, respectively. It is noted that one rod-shaped cell would incline to divide at the ring site when it contains high aspect ratio in the initial state. That is, a rod-shaped cell that possesses a higher aspect ratio, would tend to cell division more easily. The result is in well agreement with the experiments where cell division of prokaryote would be happened with respect to cell wall expansion with a constant radius[37].

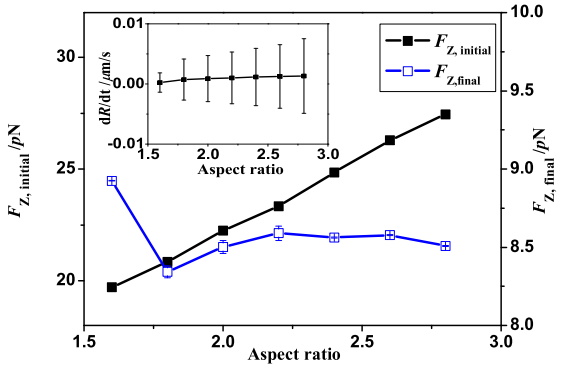

(a)

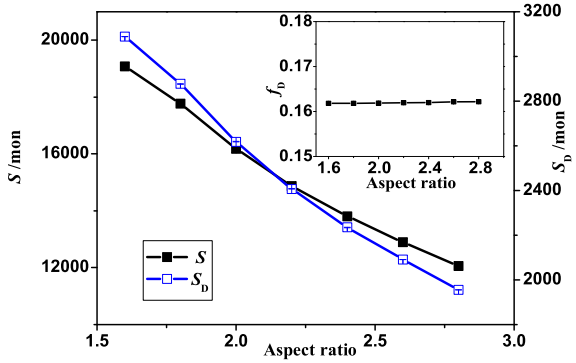

(b)

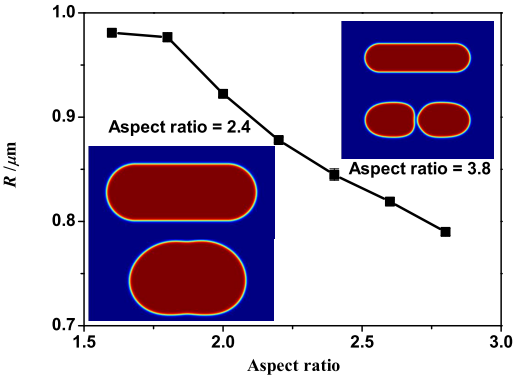

(c)

FIG. 4. (color online) . The effect of aspect ratio for rod-shaped cells, (a) constriction forces generated by FtsZ rings at the initial and steady state, and contraction rates in the inset, (b) S, S_{D} and f_{D} for FtsZ rings at the steady state, (c) The radius of midcell at the steady state, a cell shape at the initial and steady state given in the inset, respectively.

In the present study, the horizontal length of rod-shaped cells is kept a constant, while the longitude length has to adjust to satisfy with the preset aspect ratio. Therefore, the radius of rod-shaped cells, R, would reduce along with the increase of the aspect ratio, as well as the area of rod-shaped cells would respond to the transformation of the aspect ratio. If the area of rod-shaped cells with different aspect ratios is fixed, the radius of rod-shaped cell would decrease along with the increase of the aspect ratio. The initial constriction force generated by FtsZ rings would be augmented with respect to the contractile radius, when S and S_{D} are kept unchanged in the initial state, see Eq. (10). As shown in Fig. 4 (a), the initial constriction force is confirmed to increase as a function of the aspect ratio. Additionally, it can be inferred from Eqs. (13)-(14) that the total number of FtsZ and GDP-bound FtsZ monomers within the ring would be decreased along with the reduction of R in the steady state, which is confirmed in Fig. 4(b). However, the constriction force at the steady state would depend on the competition between its radius and the number of FtsZ monomers within the ring. Therefore, the forces at the steady state shown in Fig. 4(a) exhibit evidently fluctuations in response to the aspect ratio. As a whole, cell division depends on the aspect ratio for rod-shaped cells, as well as cell wall expansion *in vivo*.

Figure 5 illustrates the dependence of the dynamic process in cell divisions on the total concentration of FtsZ monomers in cells, Z_{T}, where the number of FtsZ monomers in the ring, S, is 30% of the total number of FtsZ monomers in the cell, and the fraction of hydrolyzed monomers in the ring, f_{D}, is 40 %. It is demonstrated experimentally [10,11] that at saturated FtsZ concentrations, overlapping FtsZ filaments remain, allowing additional rings to form, whereas at low FtsZ concentrations about 3-5 μM, a broad distribution of membrane-bound FtsZ monomers is observed in the midcell, but no FtsZ rings do form. A critical concentration for the ring formation is required, giving that only a single ring forms when the concentration of FtsZ monomers is about 8-10 μM, and multiple rings forms when the concentration is above 10 μM. Therefore, not only the formation of FtsZ rings but also the constriction force are expected to depend on the concentration of FtsZ monomers in cells. Figure 5(a) presents the dependences of the constriction force at the initial state and steady sate on Z_{T}. It can be seen that the constriction forces regardless of the initial and final state, $F_{\mathrm{z,initial}}$ and $F_{\mathrm{z,final}}$, increase along with the increase of Z_{T}. When Z_{T} is less than 12 μM, the constriction force generated by the FtsZ rings is found not large enough to overcome the curvature elastic energy for cells, thereby giving that the rod-shaped cell would eventually become one spherical shape

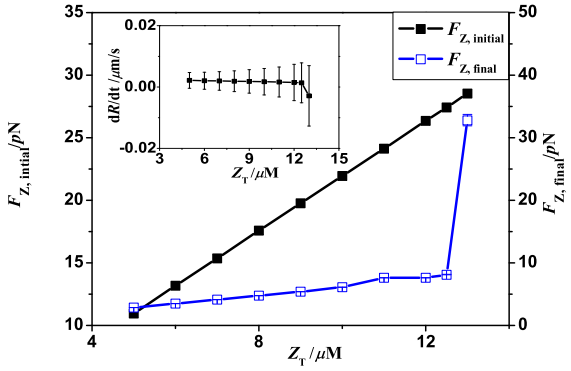

(a)

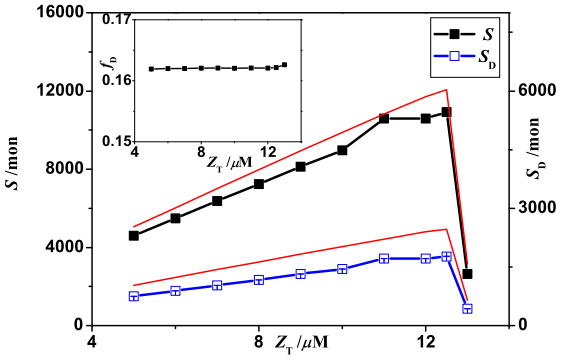

(b)

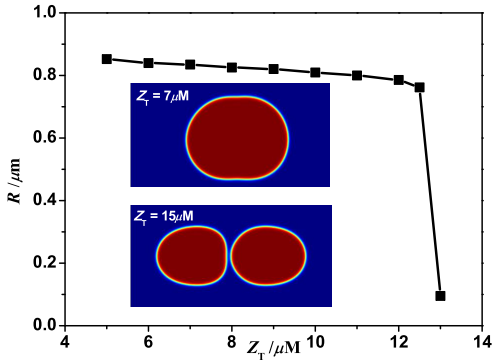

(c)

FIG. 5. (color online) . The effect of total concentrations of FtsZ monomers in cells, Z_T, (a) constriction forces generated by FtsZ rings at the initial and steady state, and contraction rates in the inset, (b) S, S_D and f_D for FtsZ rings at the steady state, the red lines are obtained from the theoretical values, Eqs. (13)-(15), (c) The radius of FtsZ rings at the steady state, a cell shape at the steady state given in the inset.

(energy benefit). As Z_{T} further increases, the cell intends to retract at the midcell, as well as the radius at the midcell becomes less. When Z_{T} increases up to 13 μM, the constriction force continuously maintains a high level, and then cell division proceeds. The radius at the midcell is presented in Fig. 5(c) as a function of Z_{T}, and the variation trend is found to be in accordance with the previous discussions. Figure 5(b) gives the dependences of the total number of FtsZ and GDP-bound monomers, S and S_{D}, on Z_{T}. It can be seen that at $Z_{\mathrm{T}} < 13$ μM, S and S_{D} would increase as a function of Z_{T}, but at $Z_{\mathrm{T}} > 13$ μM, both S and S_{D} gradually decline. Likewise, it is found that at $Z_{\mathrm{T}} > 13$ μM, cell division starts to happen, and the radius at the midcell rapidly reduces, thereby leading to the decrease of both S and S_{D}. In addition, it is found in the inset of Fig. 5(b) that the fraction of hydrolyzed monomers in the ring, f_{D}, keeps fluctuations as a function of Z_{T}, consistent with the theoretical result given in Eq. (15). At the same time, the numerical results (symbols) are found to obey with the relations of Eqs (13) and (14) (red line).

Figure 6 presents the dependence of cell morphodyanmics on the initial number of FtsZ monomers within the FtsZ rings, S_{initial}, where the initial fraction of hydrolyzed monomers in the ring, f_{D}, is still kept to 40 % . It can be seen from Fig. 6(a) that the initial constriction force generated by FtsZ rings increases linearly as a function of S_{initial}, as concluded from Eq. (10). However, we find that at $S_{\mathrm{initial}} < 6500$ monomers, the constriction force, S, S_{D} and R in the steady state are independent of S_{initial}, where the constriction force about 8.4 pN at the steady state is far less than the force required for cell division. At $S_{\mathrm{initial}} > 6500$ monomers, the initial force (about 28 pN) is larger than the critical force for cell division, the rod-shaped cell gradually shrinks at the midcell, and then cell division begins. In addition, the fraction of hydrolyzed monomers in the ring, f_{D}, is found close to 0.162$\pm$0.002 and independent of S_{initial}, see the inset of Fig. 6(b).

Figure 7 gives the effect of the initial number of GDP-bound FtsZ monomers within the ring, $S_{\mathrm{D,\ initial}}$, on cell morphodyanmics, where Z_{T} and S_{initial} are chosen as 13 μM and 6500 monomers, respectively. In Fig. 7(a), the initial constriction force generated by FtsZ ring, $F_{\mathrm{z,initial}}$, is found to increase linearly along with the enhancement of $S_{\mathrm{D,\ initial}}$. This change trend obeys with the relation of Eq. (10). Likewise, it is also found that at $S_{\mathrm{D,\ initial}} < 2600$ monomer, the constriction force, S, S_{D} and R in the steady state keep almost unchanged, and are independent of $S_{\mathrm{D,\ initial}}$, where the constriction force is about 8.4 pN and far less

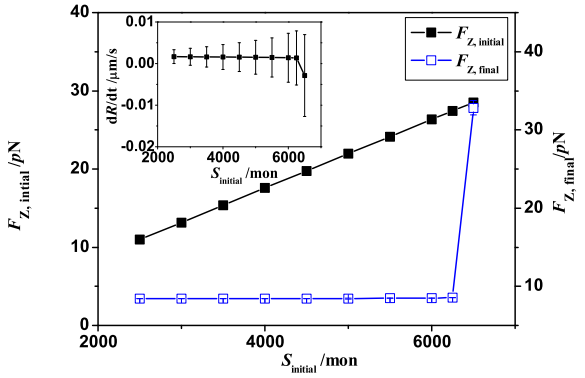

(a)

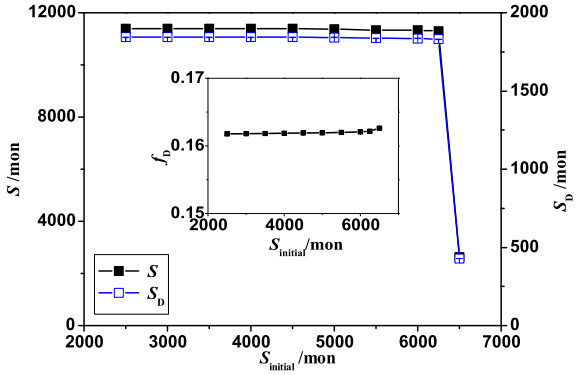

(b)

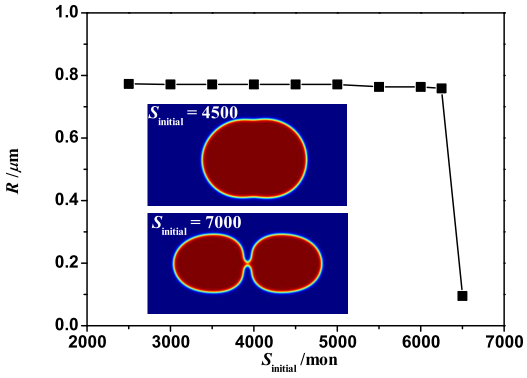

(c)

FIG. 6. (color online). The effect of the initial number of monomers in the FtsZ rings, S_{initial}, (a) constriction forces generated by FtsZ rings at the initial and steady state, and contraction rates in the inset, (b) S, S_{D} and f_{D} for FtsZ rings at the steady state, (c) The radius of constriction rings at the steady state, a cell shape at the steady state given in the inset.

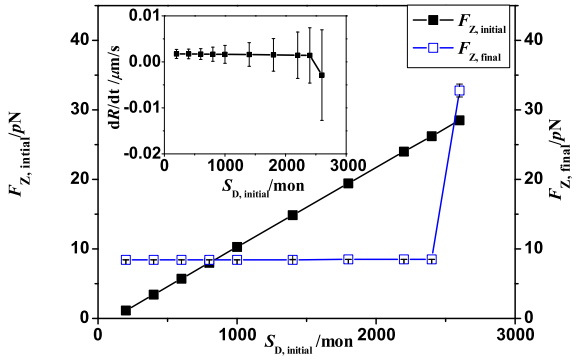

(a)

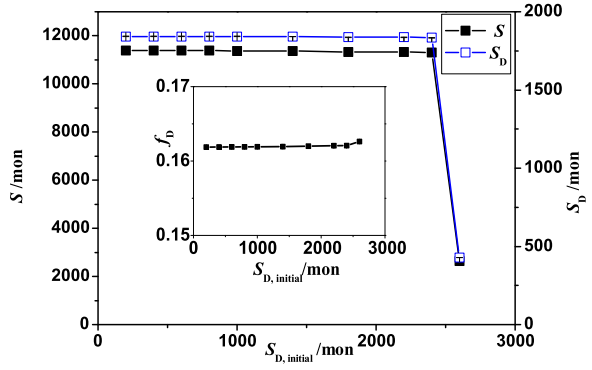

(b)

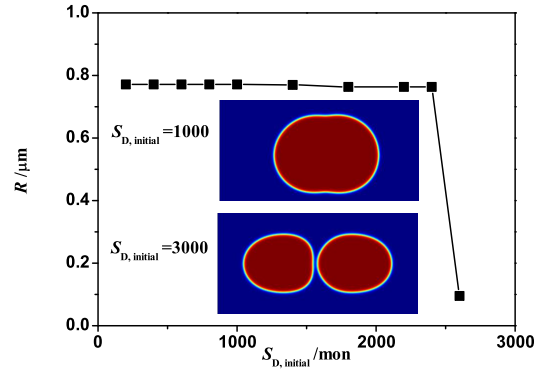

(c)

FIG. 7. (color online). The effect of the initial number of GDP-bound FtsZ monomers in the FtsZ rings, $S_{\mathrm{D,initial}}$ (a) constriction forces generated by FtsZ rings at the initial and steady state, and contraction rates in the inset, (b) S, S_{D} and f_{D} for FtsZ rings at the steady state, (c) The radius of constriction rings at the steady state, a cell shape at the steady state given in the inset.

than the critical force ($\sim$28 pN) for cell divisions. At $S_{\mathrm{D,\ initial}} > 2600$ monomers, the initial force is about 28 pN, close to the critical force for cell division. The radius at the midcell becomes much less, and then cell division is under the way. In addition, the fraction of hydrolyzed monomers in the ring, f_{D}, is found approximately to 0.162$\pm$0.002 regardless of the alteration in $S_{\mathrm{D,\ initial}}$, see the inset of Fig. 7(b).

As a result, the constriction force generated by FtsZ rings whether in the initial or in the steady state is required above the critical force 28 pN in order to arrive at cell division, regardless of the changes in the total concentration of FtsZ monomers in cells, the mean length of FtsZ filaments, and the aspect ratio for rod-shaped cells. This critical constriction force has the same magnitude with the previous result that cell division can succeed for a wide range of FtsZ rings force between 8 pN and 80 pN[25]. Additionally, it is found that when the initial constriction force generated is less than the critical force, the constriction forces, S, S_{D}, f_{D} and radius at mid-cells in the steady state are independent of the initial number of FtsZ monomers and GDP-bound FtsZ monomers in the FtsZ rings, $S_{\mathrm{\ initial}}$ and $S_{\mathrm{D,\ initial}}$. However, except the mean length of FtsZ filaments, the initial constriction forces, $F_{\mathrm{z,initial}}$, are found to increase along with the enhancement of Z_{T}, the aspect ratio for rod-shaped cells, $S_{\mathrm{\ initial}}$ and $S_{\mathrm{D,\ initial}}$. In addition, it is noted that S and S_{D} to some extent start to decrease at the beginning of such a reduction of the radius at the midcell. At the same time, the fraction of hydrolyzed monomers in the steady state, f_{D} is observed to be dependent of the mean length of FtsZ filaments, λ, but independent of Z_{T}, the aspect ratio for rod-shaped cells, $S_{\mathrm{\ initial}}$ and $S_{\mathrm{D,\ initial}}$. Whereas, S and S_{D} in the steady state are observed to depend on λ, Z_{T} and radius at the midcell, R. As a whole, these changes in S, S_{D} and f_{D} obtained in the numerical calculations are found to agree well with the theoretical results derived from Eqs. (13)-(15) that describe the quasi-steady state of the FtsZ ring subsystem.

C. Phase diagram

In *in vitro* experiments, the concentration of FtsZ monomers in cells and the aspect ratio for rod-shaped cells are observed to be different in a variety of biological processes due to cell wall expansion and protein synthesis[36]. In order to explicitly elucidate the relevance of cell division to the concentration of FtsZ

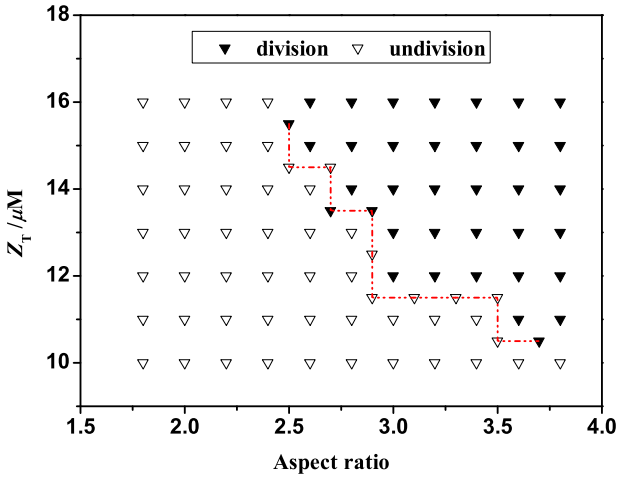

FIG. 8. (color online). Phase diagram as a function of aspect ratio for rod-shape cells and total concentrations of FtsZ in cells, Z_{T}.

monomers in cells, Z_{T}, and the aspect ratio for rod-shaped cells, phase diagram is presented in Fig. 8 that describes the steady state of rod-shaped cells, where division and undivision are employed to describe the final state of cells. It is found that when the total concentration is less than 10 μM, rod-shaped cells even with the aspect ratio high up to 3.8 can not realize cell division. It is previously reported[10,11] that only a single ring is experimentally observed to form when FtsZ concentrations is in the range from 8 to 10 μM. Therefore, the constriction force generated by a single ring is not large enough to attain the critical force for cell division. In addition, we find that cell division would be easily realized along with the increase of the concentration, Z_{T}, even with much less aspect ratio. Therefore, we can conclude that one rod-shaped cell with high aspect ratio or/and Z_{T}, is prone to divide.

IV. SUMMARY AND OUTLOOK

We have developed one new theoretical framework by a combination of phase field model for cells and a kinetics description for FtsZ ring maintenance to understand shape transformations and mechanics of dividing a rod-shaped cell. The kinetic description of dynamic FtsZ ring takes GTP-bound monomers

in the ring into account. The dynamic turnover of FtsZ rings therefore includes the association of short filaments or free monomers in the cytoplasimc pool to the ring, GTP-bound FtsZ monomers hydrolyzed to GDP-bound FtsZ ones in the ring, rapidly nucleotide exchange in the cytoplasimc pool, and detachments of both GTP-bound and GDP-bound FtsZ monomer at filament tips in the ring. The difference in the mechanical characterization of GTP-bound and GDP-bound monomers within the FtsZ ring would reflect the transformation changes of FtsZ monomers due to GTP hydrolysis. Cell divisions are determined by cooperation of the constriction force generated by dynamic FtsZ rings, the bending elastic energy and cell wall expansion.

The constriction force generated by FtsZ rings determines the contractile direction, velocity, as well as cell shape. The constriction force presented here would be altered along with the dynamic process during cell division, as well as the changes in cell shapes and dynamic turnover of FtsZ rings. We find that with reasonable parameters given in Tab. I, a rod-shaped cell would retract at the midcell when the constriction force are above the critical force about 28 pN that has the same magnitude with the previous report[25]. Cell shapes and cell division time obtained in our calculations are all comparable to physiologically observed results[11]. FtsZ filaments within the ring are also found to obey with an exponential distribution that has its characteristic length, close to the preset mean length of FtsZ filaments, λ. Likewise, cell morphodynamics during cell division are extensively investigated as functions of different initial states of rod-shaped cells and FtsZ rings, such as the aspect ratio, the mean length of FtsZ filaments, the concentration of FtsZ monomers in cells, Z_{T}, the total number of FtsZ and GDP-bound FtsZ monomers within the ring. It is found that with the increase of the aspect ratio, the mean length of FtsZ filaments, and Z_{T} in the initial state, rod-shaped cells would contract at the midcell and eventually divide when the constriction force is above the force required to cell division. However, when the constriction force is below the critical force, the cell shape attains eventually close to one spherical shape, and is independent of the total number of FtsZ and GDP-bound FtsZ monomers within the ring in the initial sate. It is noted that the total number of FtsZ and GDP-bound FtsZ monomers within the ring, S and S_{D}, to some extent start to reduce at the beginning of the reduction of the radius at the midcell. In addition, the quasi-steady state for the dynamic turnover of FtsZ rings is derived, thereby giving the theoretical expressions for S_{qss}, S_{Dqss} and f_{Dqss}, see Eqs. (13)-(15). The obtained results for S, S_{D} and f_{D} in the numerical calculations are found to be in well consistent with

the theoretical results, as well as f_{D} approaches the experimental value about 20%[11].

In order to explicitly elucidate the relation of cell division and some parameters, morphological phase diagram is presented as functions of the FtsZ concentration in cells, Z_{T}, and the aspect ratio of rod-shaped cells, giving that cell division tends to be observed in rod-shaped cells with high Z_{T} or/and high aspect ratio. As experimentally observed[10,11], only a single ring forms at $Z_{\mathrm{T}} < 10$ μM, but at this concentration, the constriction force generated by a single ring is not high enough to implement cell division. Likewise, one rod-shaped cell that possesses a higher aspect ratio, would easily cell division, which is in well agreement with the experimental result that cell division of prokaryote would be happened with respect to cell wall expansion with a constant radius[37]. Therefore, the theoretical framework presented here can effectively predict cell morphodynamics during cell division with the coupling of dynamic FtsZ ring and cell morphology.

In the present work, the dependences of cell morphodynamics during cell division on different initial states of cells and FtsZ rings are focused. Likewise, a more detailed discussion relevant to various kinetic rates within the FtsZ ring and division times would be presented in the future work. The basic theoretical framework developed here that has the evident advantage to integrate the cell shape with dynamic FtsZ rings, can be extended to study division in eukaryotic cells, such as budding and fission yeast and plant cells, which can provide valuable insights into critical cellular functions. In future research, it is also of great interests to develop other space dependent theoretical framework aimed to study the spatial structure and dynamic turnover of FtsZ rings.

ACKNOWLEDGMENTS

The financial supports of this work are provided by the Fundamental Research Funds for the Central Universities, the National Natural Science Foundation of China (Grant No. 21274038).

[1] J. Lutkenhaus Annu. Rev. Biochem. **76**, 539 (2007).

[2] P. De. Boer, R. Crossley, L. Rothfield Nature **359**, 254 (1992).

[3] D. RayChaudhuri, J. T. Park, Nature **359**, 251 (1992).

[4] Mukherjee A, Lutkenhaus J EMBO J. **17**, 462 (1998).

[5] L. Romberg, M. Simon, H. Erickson, J. Biol. Chem. **276**, 11743 (2001).

[6] M. A. Oliva, S. Huecas, J. M. Palacios, J. Martin, J. M. Valpuesta, J. Biol. Chem. **278**, 33562 (2003).

[7] H. Erickson, D. Taylor, K. A. Taylor, Proc. Natl. Acad. Sci. USA **93**, 519 (1996).

[8] S. Sharma, H. Zhu etc., Nanoscale **5**, 5692 (2013).

[9] J. M. gonzalez, M. Jimenez, J. Mingorance, J. Biol. Chem. **278**, 37664 (2003).

[10] Anderson D, Gueiros-Filho F., Erickson H J. Bacteriol. **186**, 5775 (2004).

[11] H. P. Erichson, D. E. Anderson, M. Osawa Microbio. Mol. Rev. **74**, 504 (2010).

[12] H. P. Erichson Proc. Nat.l Acad. Sci. USA **106**, 92383 (2009).

[13] J. F. Allard, E. N. Cytrynbaum Proc. Natl. Acad. Sci. USA **106**, 145 (2009).

[14] K. K. Guo, J. Shillcock, R. Lipowsky, J. Chem. Phys. **133**, 155105 (2010).

[15] K. K. Guo, W. J. Xiao, D. Qiu, J. Chem. Phys. **135**, 105101 (2011)

[16] J. Stricker, P. Maddox, E. D. Salmon, H. P. Erickson, Proc. Natl. Acad. Sci. USA **99**, 3171 (2002).

[17] M. A. Oliva, S. C. Cordell, Nat. Struct. Mol. Biol. **11**, 1243 (2004)

[18] J. Hsin, A. Gopinathan, K. C. Huang Proc. Natl. Acad. Sci. USA **109**, 9432 (2012).

[19] M. Osawa, H. P. Erickson, EMBO J. **28**, 3476 (2009).

[20] M. Osawa, D. E. Anderson, H. P. Erickson Science **320** 792 (2008).

[21] G. H. Lan, B. R. Daniels, T. M. Dobrowsky, D. Wirtz, S. X. Sun Proc. Natl. Acad. Sci. USA **106**, 121 (2009).

[22] G. H. Lan, A. Dajkovic, S. X. Sun Biophys. J. **95**, 4045 (2008).

[23] Y. G. Shu. Z. C. Ou-Yang Nanoscale **2**, 1284 (2010).

[24] B. Ghosh, A. Sain Phys. Rev. Lett. **101**, 178101 (2008).

[25] G. Lan, C. Wolgemuth, S. Sun Proc. Natl. Acad. Sci. USA **104** , 16110 (2007).

[26] R. Folch, J. Casademunt, A. H. Machado, Phys. Rev. E. **60**, 1724 (1999).

[27] T. Biben, K. Kassner, C. Misbah, Phys. Rev. E. **72**, 041921 (2005).

[28] J. S. Lowengrub, A. Ratz, A. Voigt, Phys. Rev. E. **79**, 031926 (2009).

[29] Q. Du, C. Liu, X. Wang, J. Comput. Phys. **212**, 757 (2006).

[30] D. Y. Shao, W. J. Rappel, H. Levin Phys. Rev. Lett. **105**, 18104 (2010).

[31] Z. Liu, K. K. Guo Acta Chim. Sinica **17**, 1183 (2013).

[32] W. J. Xiao, K. K. Guo Soft Matter **10**, 2539 (2014).

[33] K. Keren, Nature **453**, 475 (2008).

[34] L. Landau, L. Pitaevskii, E. Lifshitz, Theory of Elasticity, Pergamon Press (1986).

[35] A. Dajkovic, G. Lan, S. Sun, D. Wirtz, J. Lutkenhaus Curr. Biol. **18**, 235 (2008).

[36] J. Maennik, F. B. Wu, F. J. H. Hol, Pl Bisicchia et. al. Proc. Natl. Acad. Sci. USA **109**, 6957 (2012).

[37] E. C. Garner, Science **333**, 222 (2011).